Journal of Materials Chemistry

www.rsc.org/materials

Volume 20 | Number 8 | 28 February 2010 | Pages 1389–1608

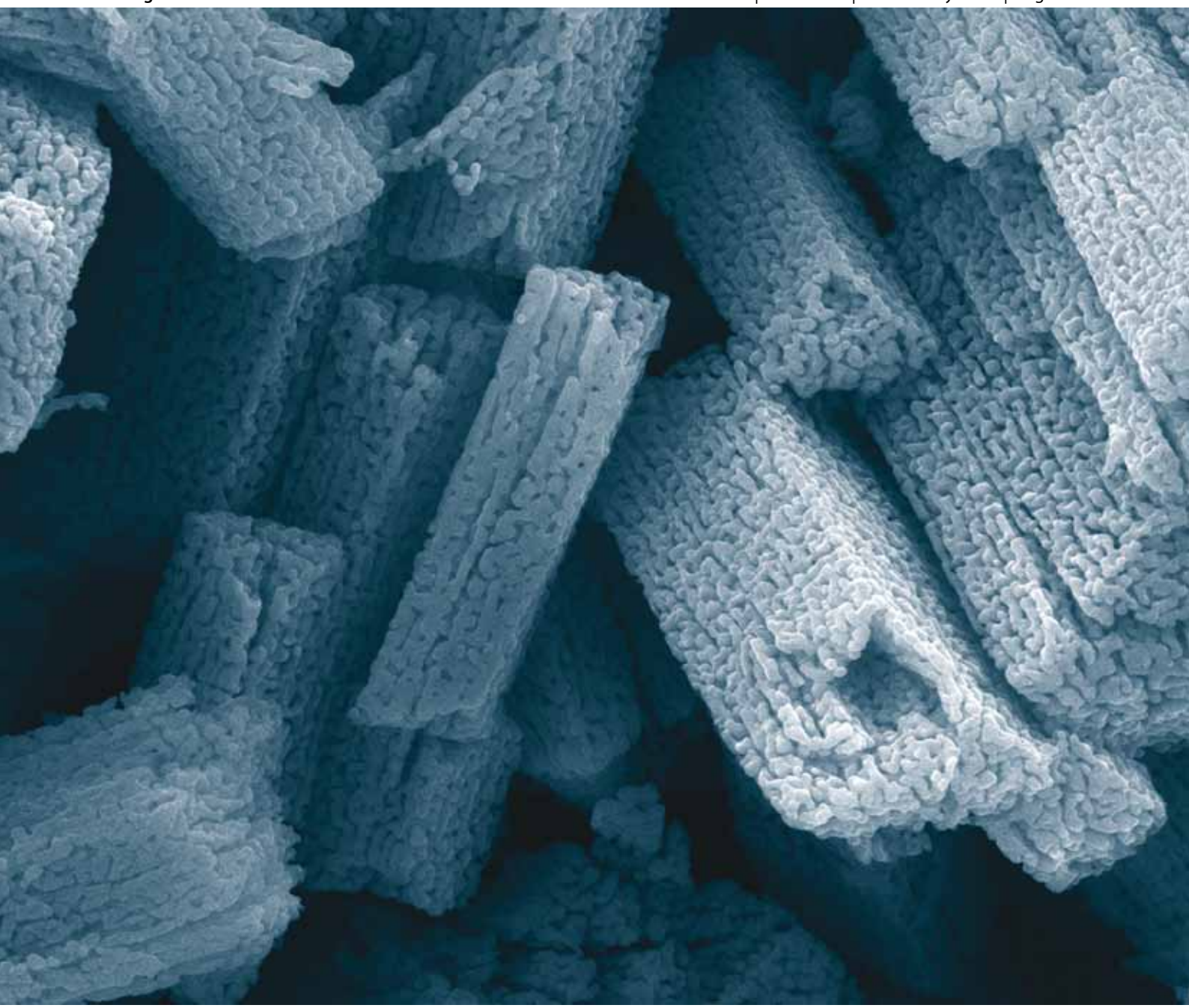

ISSN 0959-9428

RSC Publishing

0959-9428(2010)20:8;1-3

Spontaneously formed porous and composite materials

Serena A. Corr,[*a] Daniel P. Shoemaker,[a] Eric S. Toberer[b] and Ram Seshadri[ac]

Received 31st July 2009, Accepted 29th October 2009
First published as an Advance Article on the web 10th December 2009
DOI: 10.1039/b915613e

In recent years, a number of routes to porous materials have been developed which do not involve the use of pre-formed templates or structure-directing agents. These routes are usually spontaneous, meaning they are thermodynamically downhill. Kinetic control, deriving from slow diffusion of certain species in the solid state, allows metastable porous morphologies rather than dense materials to be obtained. While the porous structures so formed are random, the average architectural features can be well-defined, and the porosity is usually highly interconnected. The routes are applicable to a broad range of functional inorganic materials. Consequently, the porous architectures have uses in energy transduction and storage, chemical sensing, catalysis, and photoelectrochemistry. This is in addition to more straightforward uses deriving from the pore structure, such as in filtration, as a structural material, or as a cell-growth scaffold. In this feature article, some of the methods for the creation of porous materials are described, including shape-conserving routes that lead to hierarchical macro/mesoporous architectures. In some of the preparations, the resulting mesopores are aligned locally with certain crystallographic directions. The coupling between morphology and crystallography provides a macroscopic handle on nanoscale structure. Extension of these routes to create biphasic composite materials are also described.

Introduction

Porous materials are vital in a wide range of applications, including catalytic materials, filters, sensors, batteries, photovoltaics, fuel cells, and optical devices. Many of these applications require extensive fluid–solid contact which porous architectures can provide. In developing families of routes to form porous materials, control over both pore wall composition and morphology is sought. Pore wall composition dictates the stability, reactivity, and intrinsic material properties such as piezoelectricity, catalytic activity, magnetism, or conductivity. The morphology influences surface area, strength, and the rate of fluid exchange through the pores.

For example, porous semiconducting metal oxides find uses as gas sensing materials since the interaction of gas molecules with the porous surface produces measurable changes in the electrical conductivity.[1] Porous materials are attractive for photocatalysis,

[a]*Materials Department and Materials Research Laboratory, University of California, Santa Barbara, CA 93106, USA. E-mail: serena@mrl.ucsb.edu; Fax: +1 (805) 893 8797*
[b]*Materials Science, California Institute of Technology, Pasadena, CA 91125*
[c]*Department of Chemistry and Biochemistry, University of California, Santa Barbara, CA 93106, USA*

Serena A. Corr

Serena Corr is a Lecturer in Materials Research at the University of Kent, UK. She obtained her BA (2002) and PhD (2007) in Chemistry from Trinity College Dublin, before working as a postdoctoral researcher at the University of California, Santa Barbara with Professor Ram Seshadri. Her research focuses on functional nanostructured materials and their many uses, in particular exploring the physical properties of metal oxides for their potential use in medical, electronic and energy applications.

Daniel P. Shoemaker

Daniel Shoemaker is a fourth-year graduate student in the Seshadri group in the Materials Department at the University of California, Santa Barbara. Daniel received his BSc with Honors in 2006 from the Materials Science and Engineering Department at the University of Illinois, Urbana-Champaign. His research focuses on structure–processing–property relations in oxides with structural and compositional disorder on the nanoscale. This includes magnetic characterization of spontaneously formed composites and total neutron scattering studies of single-phase materials with non-cooperative atomic distortions.

since porosity minimizes the distance between the site of photon absorption and electron/hole redox reactions, thereby enhancing efficiency.[2,3] The large specific areas associated with porous materials make them good candidates for cathode materials since this can lead to higher current density, and the length of intercalated ionic diffusion paths can be reduced due to the material's thin pore walls.[4]

Porous materials are frequently prepared using pre-formed templates or structure-directing agents. The use of templates provides many advantages. The choice of template can be tailored to provide exotic and complex structures. To consider a few recent examples, mesoporous silica (SBA-15), itself prepared using a template, has been used as a template to generate other materials with well-ordered channels and a variety of pore diameters.[5] Hierarchically porous structures of silica, niobia, and titania have also been prepared by the combination of structure-directing block copolymers, latex sphere templates, and metal alkoxide precursors.[6] Biomineral templates, in the form of sea urchins, which have been sacrificed after deposition, yield porous gold, nickel, titania and silica structures.[7,8] Eggshell membranes have also been used as hosts to prepare organized hierarchical structures of ZnO, Co_3O_4, PdO and TiO_2.[9,10] Other templates which have been used for the preparation of porous materials include layered double hydroxides,[11] dextrans,[12] silica monoliths and spheres,[13–15] neutral or charged surfactants,[16] emulsion templating,[17,18] activated carbon fibers,[19] and amino acids,[20] to name but a few. A recent review article on porous materials deals specifically with templated synthesis.[21]

The focus of this feature is however on routes that do not require pre-formed templates. Such routes avoid the waste and cost associated with first forming a template and then destroying it to obtain the final material. In addition, post-preparative template removal can lead to shrinkage of the porous frameworks and a loss of the desired porosity. The use of templates makes the scaling-up of preparations an obstacle. Samples prepared by template-free methods also frequently possess higher thermal stability in comparison to their template-prepared counterparts.[3] In a previous review, we addressed some of the early efforts at template-free routes to porous inorganic materials.[22] Since then, there has been a great deal of work focused on spontaneously formed porous materials. Here, we concentrate on spontaneous processes which yield porous and composite materials. One of the goals of the work has been to prepare functional metal oxide materials with controlled porosity. In particular, our recent work has focused on the preparation of hierarchically porous materials. In this feature article, we describe the latest developments in the preparation of spontaneously formed porous and composite materials.

Porous materials

Selective leaching in ceramics

Work from Santa Barbara on spontaneously formed porous materials has taken advantage of a selective leaching process. Intimately-mixed two-phase composites have been prepared, one of which acts a sacrificial phase, leaving behind a porous monolith of the desired phase upon leaching. Inspiration for using this method stemmed from the preparation of porous Vycor™ glass. Here, a single-phase borosilicate glass undergoes a spinodal decomposition to give regions of borosilicate-rich and poor glass on the nanometre scale. Leaching of the boron-rich phase leaves behind a monolith of porous glass.[23] A major advantage to employing this route is the fact that, by careful consideration of the chemistry of the mixed composite, a strategy may be designed for the preparation of a desired porous material. The initial concern when designing these experiments is that the two starting metals do not react together to form oxides or a solid solution. Also, it should be possible to selectively remove one phase, without any deleterious effects on the other. By preparing a single-source two-component precursor which contains both metals, one can simply press a pellet of the material, decompose and sinter it and leach out the sacrificial phase to be left with a macroporous monolith of the required phase.

Mixed composites can be prepared using a variety of methods, including decomposition of precipitated hydroxy double salts, combustion synthesis, and decomposition of mixed metal oxalates. For example, we have used the combustion synthesis route to prepare an intimate mixture of NiO and ZnO, which was

Eric S. Toberer

Eric S. Toberer is a Beckman Postdoctoral Fellow in Materials Science at the California Institute of Technology. Eric conducted his graduate work with Ram Seshadri at the University of California, Santa Barbara (2002–2006) on the synthesis of porous materials. His research interests in the spontaneous formation of nanostructures have led to research on thermoelectric materials, where he has developed bulk nanocomposites to control electron and phonon transport.

Ram Seshadri

Ram Seshadri is Professor of Materials, and Professor in the Department of Chemistry and Biochemistry at the University of California, Santa Barbara. Prior to starting at UCSB, Ram was Assistant Professor at the Indian Institute of Science, Bangalore (1999–2002). His research addresses the theme of structure–morphology–property relations in crystalline inorganic compounds, and especially those displaying interesting catalytic, electronic, magnetic, optical, and polar properties. Since January 2009, Ram has served as one of two US Associate Editors for this journal.

then sintered.[24] Alkali treatment removes the ZnO phase, leaving a porous monolith of NiO which, upon reduction in 5% H_2, can be transformed to the pure metal. Decomposition of the hydroxyacetate precursor, $Ni_3Zn_2(OH)_8(CH_3COO)_2 \cdot 2H_2O$, also yields a mixture of NiO and ZnO. Alkali leaching selectively dissolves the zinc oxide, and after a reduction step pure, porous Ni is obtained.[25] Taking this process a step further, we have used ZnO as a sacrificial phase for the formation of porous $Ni_{0:7}Zn_{0:3}O$ and $ZnFe_2O_4$ monoliths. Porous monoliths of elemental metals, Ni and Fe respectively, can be then prepared by subsequent reduction of the oxides. We have also looked at the surface reactivity of the nickel oxide and found that the Ruddlesden–Popper phase, $La_4Ni_3O_{10}$, can be prepared by simply coating with a lanthanum source and heating.[26]

These one-pot preparations, which allow for the formation of two daughter phases – one to be sacrificed and the other the desired material – provide a relatively straightforward method for the preparation of more complex porous materials. However, care must be taken when designing these experiments. If the grains of the phase to be sacrificed are much larger than the desired phase, leaching will result in the formation of large, isolated pores. If the opposite is true and the grains of the desired phase are much larger than the sacrificial phase, there will be limited connectivity between grains in the desired phase, and the resulting monolith will be susceptible to cracking.

Exploitation of inorganic reaction pathways also allows for the preparation of macroporous monoliths of functional materials. Our early venture into the use of this method allowed us to prepare $PbZrO_3$ at relatively low temperatures from the metathetic exchange reaction between $PbSO_4$, ZrO_2 and K_2CO_3.[27] Our hope was that with the elimination of the corresponding K_2SO_4, we could prepare a porous network. While this aim was not achieved here, further exploration of this route has allowed us to prepare porous perovskites $PbTiO_3$ and $La_{1-x}Sr_xMnO_3$ ($x = 0.0$ and 0.3) at reduced temperatures in a similar manner.[28] The dissolution of the resulting sulfate species by immersing a pellet of the material in water results in the preparation of macroporous monoliths. Mechanical robustness of the monoliths is improved by sintering at 1048 K.

The porosity and pore size can be controlled by the proportion and grain size of the soluble phase. For example, the perovskite material $La_{0:8}Sr_{0:2}FeO_{3-\delta}$, which attracts attention due to its potential application as cathode material in solid oxide fuel cells, can be prepared in the form of a porous network by using sodium carbonate as the soluble phase.[29] Sodium carbonate was found to render the ceramic material porous, with smaller pore sizes of 200 nm found from electron microscopy studies.

Sublimation of a phase, instead of dissolution, can likewise generate porosity. For example, a recent paper reports the preparation of highly porous CeO_2.[30] Ceria materials have important potential applications in solid-state electrochemistry. To generate porous CeO_2, an intimate mixture of CeO_2 and SnO_2 was prepared. The use of SnO_2 as the pore-forming material is advantageous for a number of reasons. It is immiscible with CeO_2 and will not affect the crystal structure or catalytic properties of the CeO_2. Also, since the melting point of SnO_2 is near the firing temperature of CeO_2, the sacrificial component may be removed by sublimation, without the need for subsequent leaching or reduction steps.

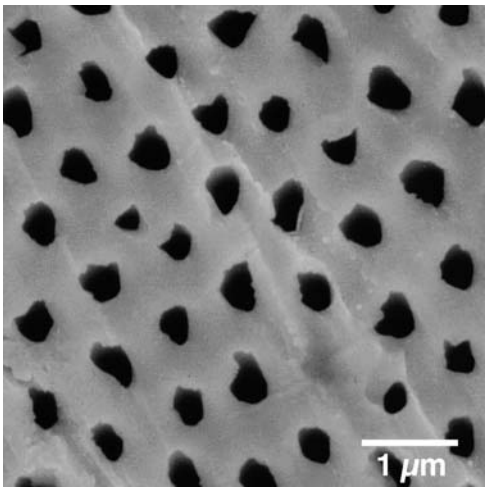

Fig. 1 Unidirectionally porous ZrO_2 prepared by selectively etching MgO from a cooled ZrO_2–MgO eutectic mixture. Scanning electron microscopy (SEM) image showing uniformly distributed pores, with a typical diameter of 300 nm. Image provided by Y. Suzuki, as described in ref. 32.

One can also take advantage of the structure of the parent precursor material. For example, layered double hydroxides (LDHs), a class of synthetic anionic clays, are made up of two-dimensional brucite-type layers held together *via* the electrostatic interactions between interlayer anions and positively charged layers. Calcination of these materials allows for the formation of spinels, together with the oxide of the divalent metal. By exploiting this fact, Zou *et al.* have prepared two-phase materials made up of the desired phase and MgO from the high temperature sintering of LDH precursors.[31] The MgO phase may be removed by dissolution in $(NH_4)_2SO_4$ solution at 80 °C. In this manner, porous monoliths of $MgAl_2O_4$, $MgAl_2O_4$ and $In_{2-x}Mg_xO_3$ have been prepared which display promising surface superhydrophobicity, ferromagnetic and semiconductor properties, respectively.

Unidirectionally porous cubic ZrO_2 has been prepared by Suzuki and coworkers.[32] By careful consideration of the ZrO_2–MgO phase diagram, a cubic zirconia solid solution was prepared, which was rendered porous by acid etching of the MgO component. Sintered samples of a ZrO_2-MgO composite were melted and solidified. The uniformity and directionality of the sample is due to the local temperature gradient of the melt (see Fig. 1). Suzuki *et al.* have also prepared porous $CaZrO_3/MgO$[33] and $CaZrO_3/MgAl_2O_4$ composites using natural dolomite $[CaMg(CO_3)_2]$ as a starting material to react with zirconia with 0.5% LiF incorporation. In these reactions, the CO_2 gas liberated during the reaction disrupts the densification process leading to a unique 3D microstructure. The LiF lowers the decomposition temperature of the dolomite and serves to speed up the reaction. As it is molten during the reaction, LiF also wets the oxide particles, promoting the formation of strong necks between the particles, resulting in a 3D network.

Dealloying of metals

The work in dealloying and leaching of ceramics has been strongly influenced by both past as well as more recent work on

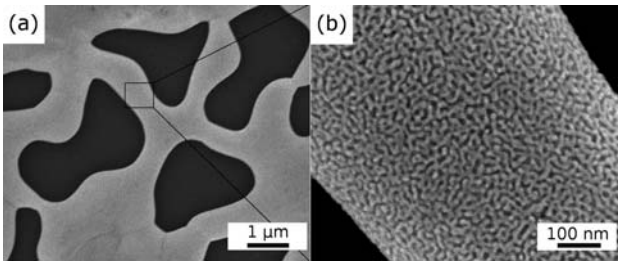

Fig. 2 Images displaying the bimodal porosity in nanoporous gold, taken from ref. 38. A white gold leaf, 100 nm thick, yields nanoporous gold upon dealloying the silver component. The larger pores in (a) result from an annealing step. Re-plating with silver and dealloying gives the mesoporous structure (b). Reproduced with permission from ref. 38. © 2003, American Chemical Society.

metals. The dealloying mechanism involves a phase separation at the solid–liquid interface, with the dissolution of a species.[34,35] It is an inexpensive route to porous metals, and can be tailored to provide a desired product. The best known example of selective leaching is the preparation of RANEY® nickel catalysts, which occurs by the leaching of aluminium from Ni–Al alloys.[36]

Using a dealloying or metallic corrosion technique, Erlebacher and coworkers have prepared nanoporous gold from a gold–silver alloy by selective dissolution of the silver.[37] Monte Carlo methods have allowed for the modeling of this dissolution process. Nanoporous gold can also prepared by dealloying commercially available white gold leaf. Subsequent treatments of these porous membranes have provided a number of interesting new materials. Bimodal porosity may be achieved by coarsening the pores through annealing at elevated temperatures, followed by re-plating with silver and a second cycle of annealling and dealloying (see Fig. 2).[38]

In order to prepare nanoporous copper for surface-enhanced Raman scattering applications, Chen and coworkers have examined $Cu_{30}Mn_{70}$ as a precursor since the large electrochemical potential difference should allow for the straightforward dealloying of the manganese component.[39] By studying the binary Cu–Mn phase diagram, these authors predicted that a single-phase Cu–Mn alloy could be prepared by rapid cooling from high temperatures. Etching of the manganese entity was achieved using hydrochloric acid. However, one must take care at this point since the homogeneity and stability of the nanoporosity depends on the acid concentration. Coarsening of the pores may be controlled by increasing the dealloying time. For example, the average pore size was tuned from 15 nm to 120 nm by increasing the dealloying time from 0.5 to 32 h.

Reduction

Reductive transformations can also yield porous structures. Reduction of amine-templated $V_2O_{5-\delta}$ nanoscrolls affords rutile VO_2 and corundum V_2O_3 nanotubes, which are made up of porous walls with smaller, dense crystallites noted during TEM (see Fig. 3).[40,41] These porous structures are formed due to the loss of the amine intercalant, which acts as a sacrificial pore-former during the reduction process which is carried out at elevated temperatures. Fig. 3(a) shows a sample of corundum V_2O_3 which has been reduced at 600 °C for 3 h in a 5% H_2 environment. The diaphanous nature of the nanotube walls is clear from TEM and N_2 sorption measurements detail the mesoporosity of this material.

In a separate experiment, pellets of V_2O_5 powders pressed and fired at 853 K for 50 h were reduced to give V_2O_3 (see Fig. 4). SEM images, shown in Fig. 4(b) and (c), reveal pores 50 nm to 100 nm in diameter penetrating through the material. The expression of porosity was found to depend on grain size: smaller grains simply contract while larger grains become perforated with pores. This may be the result of pinning from the interior structure coupled with fairly high solid-state diffusion rates.

One class of porous materials of particular interest are those which display a hierarchy of pore sizes. Materials with pores of multiple length scales can possess a high surface area combined with a more open network of channels for improved flow rate. By the combination of several methods, namely, solid state reactivity and vapor-phase leaching, materials with a bimodal pore distribution may be obtained. For example, decomposition of the single source precursor, $Zn_{1-t}Mn_t(C_2O_4)\cdot 2H_2O$ (where t can be varied), gives an intimate mixture of wurtzite $Zn_{1-x}Mn_xO$ and the spinel-like tetragonal phase $ZnMn_2O_4$ (see Fig. 5).[42] Alkali leaching allows for the selective removal of the wurtzite phase, leaving behind a macroporous $ZnMn_2O_4$ monolith.

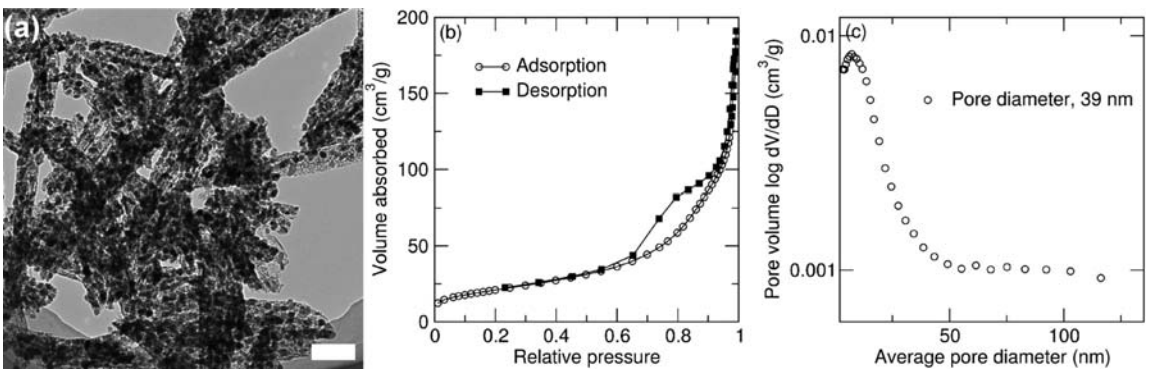

Fig. 3 (a) Transmission electron microscopy (TEM) image of porous corundum V_2O_3 formed after reduction of $V_2O_{5-\delta}$ nanoscrolls in 5% H_2 at 600 °C for 3 h (scale bar is 200 nm). The porosity of the material is evident from electron microscopy, together with a second phase of more crystalline material. (b) N_2 sorption profile and (c) corresponding pore size distribution showing the mesoporous nature of this material, with an average pore size of 39 nm noted. Details of the morphologies and transformations are described in ref. 40.

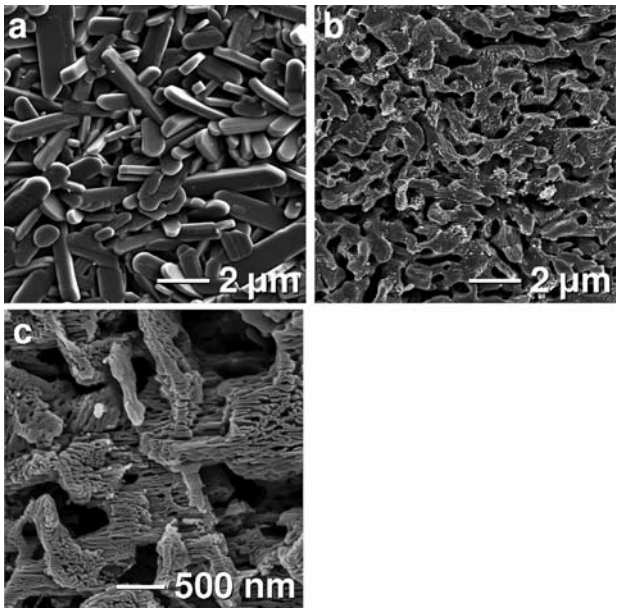

Fig. 4 SEM images of (a) sintered pellet of V_2O_5, (b) after reduction to V_2O_3, with (c) a corresponding perforation of the grains. Typical pore sizes are of the order of 50 nm to 100 nm.

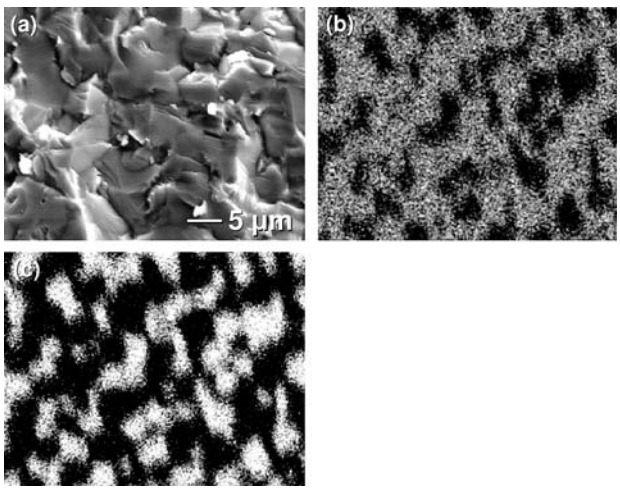

Fig. 5 EDX mapping of a dense $ZnMn_2O_4$/ZnO composite (a). The distribution of (b) Zn and (c) Mn is shown. The regions with low Mn concentrations correspond to the ZnO phase. The scale of images (b) and (c) are identical to (a).

Interestingly, reduction of this monolith by heating in flowing 5% H_2 produces an MnO monolith which displays two levels of porosity: the original macroporosity from the leaching step and now a new mesoporosity bestowed on the material by the reduction step. This reduction step facilitates the vapor-phase leaching of elemental Zn and its oxygen counterion from $ZnMn_2O_4$. Electron microscopy studies show these mesopores have right-angled edges, suggesting crystallographic control over the pore formation.[43] Further electron diffraction studies revealed that the pore morphology and pore wall crystallography were correlated, with the pore walls representing {100} crystal faces.

An analogous system to $ZnMn_2O_4$ is $SnMn_2O_4$, as the reduction of zinc and tin occur at fairly similar temperatures and both elements display low melting points (Zn: 692.9 K; Sn: 505.2 K). $SnMn_2O_4$ may be prepared by heating equimolar amounts of SnO_2 and Mn_2O_3 at 1673 K for 12 h under a N_2 atmosphere.[44] Reduction of $SnMn_2O_4$ in 5% H_2 at 923 K reduction for 12 h induced a mass loss of 10.7%, in close agreement to the 10.9% mass loss expected for the reduction to Sn metal and MnO. The resulting microstructure is shown in Fig. 6, with large droplets of Sn metal and a porous MnO structure. The droplets are found at all length scales, from 0.1 μm to 1.0 mm.

Hierarchically porous MnO can also be prepared by the direct reduction of sintered pellets of Mn_3O_4.[45] Of note here is the fact that the mesoporosity of this material is redox-reversible. Oxidation of the MnO closes the mesopores, while fresh mesopores may be generated by reduction of the material. The implications of this behavior are quite exciting when one considers the deactivation of catalysts due to the loss of surface area. Another interesting observation in this material is the shape of the mesopores. Electron microscopy studies of focused ion

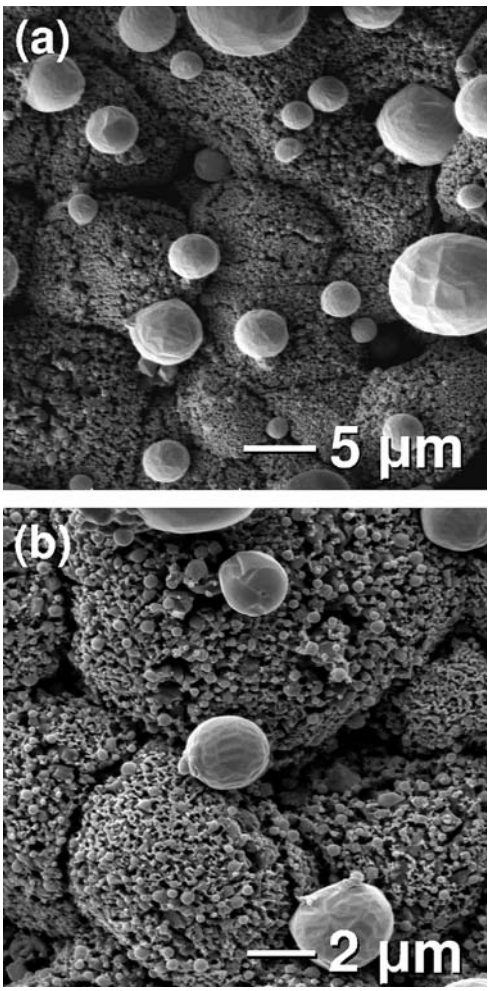

Fig. 6 (a) and (b) SEM images of MnO and Sn formed upon reduction of $SnMn_2O_4$ in 5% H_2. Unlike the case where Zn is used as a sacrificial element, where the high volatility of Zn lends itself to *in situ* removal through vapor phase leaching, Sn remains in the final composite as large particles on the surface of the porous MnO. Reproduced from ref. 44.

beam sections of this material again show the mesopores have rectangular cross-sections and self-affine and align with other mesopores, indicating their shape and orientation is determined crystallographically.

Successive leaching of phases has also allowed for the preparation of hierarchically porous rutile TiO_2 structures (see Fig. 7).[46] Reaction of ZnO with TiO_2 under oxidizing conditions at 1473 K afforded a monolith of mixed ZnO and Zn_2TiO_4. Treatment with dilute acid dissolved the ZnO phase, with a macroporous Zn_2TiO_4 phase, with pores 2 to 5 μm in size, remaining. The structural integrity of this monolith may be enhanced by sintering in air. Reduction and vapor phase leaching of the resulting Zn gave the resulting rutile TiO_2 its bimodally porous structure, with submicrometre (100–200 nm) pores developing in the macropore walls. The initial pore size was found to be in the range of 10 nm, but because of the conditions required for the complete removal of the Zn component, there is an inevitable coarsening of the pores.

The reduction of $ZnMn_2O_4$ to MnO with the Zn being distilled out, as mentioned earlier, results in the formation of porous MnO where the pores are rectangular and whose walls are all rock salt {100}.[42,43] Thus the porosity possesses a crystallographic handle that should allow control of the pore orientation in single crystals that are rendered porous. By growing epitaxial $ZnMn_2O_4$ thin films on oriented (100) and (111) substrates of spinel $MgAl_2O_4$, this idea can be tested.[47] Reduction and vapor-phase leaching of oriented $ZnMn_2O_4$ does indeed give rise to porous MnO films with all the pores oriented according to the the original orientation of the epitaxial film. This is illustrated for (100) oriented pores in Fig. 8.

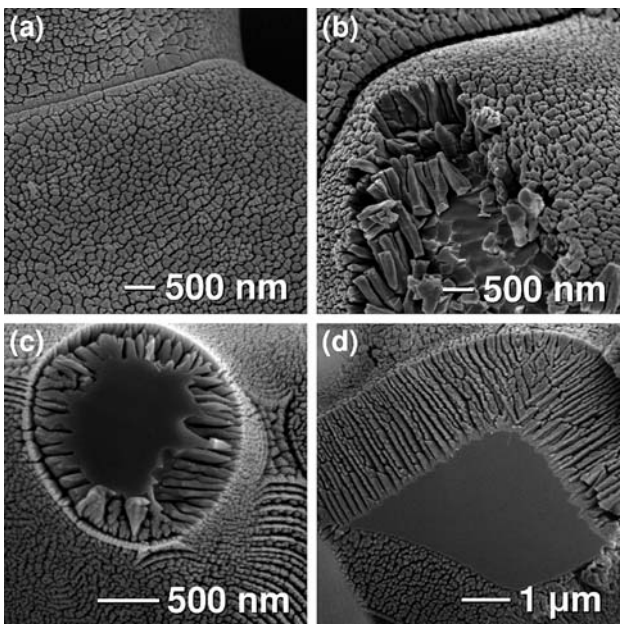

Fig. 7 SEM images of partially reduced macroporous Zn_2TiO_4, showing the development of porosity after various extents of reduction and vapor phase leaching: (a) Two grains of macroporous Zn_2TiO_4 after brief reduction. (b) Reduction and leaching lead to the formation of TiO_2 dendrites, some of which were broken to reveal the underlying dense Zn–Ti–O inverse spinel. (c) A cross-sectional view of the same sample as in (a) and (b) showing a fracture surface across a macropore wall. The dense material in the middle is again the inverse spinel. (d) A sample showing aligned TiO_2 dendrites that are representative structural features. Reproduced with permission from ref. 46. © 2006, American Chemical Society.

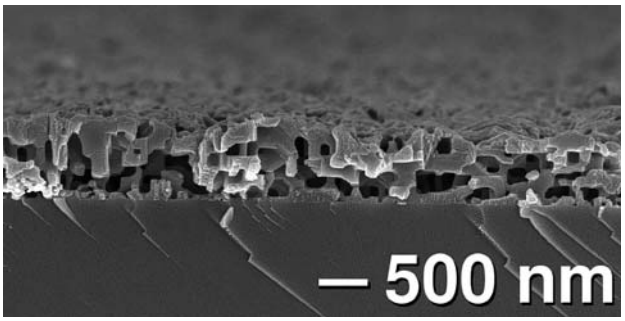

Fig. 8 SEM image of the product of reduction of an epitaxial $ZnMn_2O_4$ thin film grown on a (100) oriented spinel $MgAl_2O_4$ substrate. The resulting rock-salt MnO is perforated with rectangular holes that are all aligned with the plane of the film. Reproduced with permission from ref. 47. © 2007, American Chemical Society.

Other routes to porous ceramics

Hydrothermal treatment of precursors is a common route to porous materials. In a recent article, Ren *et al.* have prepared porous nanocrystals of a variety of manganese oxides.[48] Of particular note in this work is the uniformity and definition of the pores formed in α-Mn_2O_3 samples prepared by the calcination of a $MnOOH/Mn_3O_4$ starting material. The $MnOOH/Mn_3O_4$ mixture is made up of aggregates of manganese oxide nanoparticles, which fuse together during calcination to give uniform α-Mn_2O_3 crystals with regular mesopores (see Fig. 9).

Porous manganese oxides have also been prepared by the combination of manganese oxalate with amino acids, followed by hydrothermal treatment.[4] Calcination gave amorphous MnO_2 or crystalline Mn_2O_3, depending on the time scales involved. The

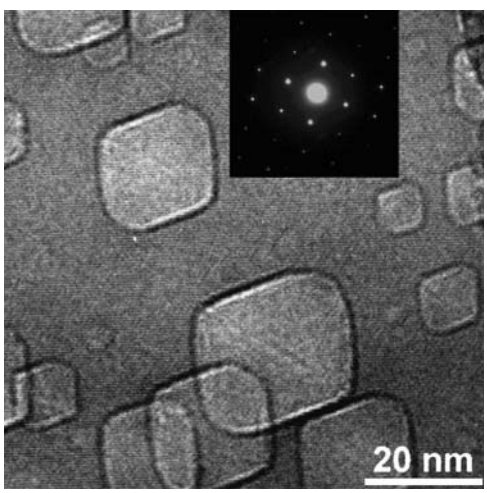

Fig. 9 TEM image of α-Mn_2O_3 hexagonal nanoplates prepared by the calcination of a $MnOOH/Mn_3O_4$ mixture. The porosity is evident, along with the crystallinity, and the striking regularity of the mesopore shape. Reproduced with permission from ref. 47. © 2008, Elsevier.

terminal functional group and length of the side chain of the amino acid employed in the preparation had a major effect on the final morphology of the products. We have also demonstrated the versatility of oxalates as precursors for the preparation of porous metal oxides, which we shall discuss in detail later.

Alkoxide hydrolysis and sol–gel methods have also been used extensively to prepare spontaneously porous metal oxide structures. In the sol–gel process, a porous network may be generated by cross-linking of the sol particles.[1] Porous anatase or rutile TiO_2 can be prepared by varying the calcination temperatures of hydrolyzed tetrabutyl titanate solutions.[3] The authors report an increase in grain size on going through the anatase-rutile phase transition above 600 °C, a fact mirrored by BET measurements which showed a decrease in the specific areas with increasing temperature. The anatase phase adopts a hierarchically porous structure with long parallel aligned macroporous channels and mesoporous channel walls. The decrease in surface area is due to the closing of these mesopores on increasing the temperature. By changing the experimental design, these authors have also prepared trimodal macro-/mesoporous titania structures.[49] By hydrothermally treating tetrabutyl titanate solutions, biphasic sponge-like macro-/mesoporous structures of anatase and brookite were obtained. Electron microscopy and N_2 sorption measurements have shown three levels of porosity: fine mesopores with average diameters of 3.7 nm to 6.9 nm, larger mesopores (23 nm to 29 nm), and macropore channels.

A two-step procedure for the formation of mesoporous TiO_2(B) nanosheets has recently been reported.[50] Here, formic acid acts as the solvent and titanium isopropoxide as the precursor. The presence of the excess carboxylic acid causes the esterification of the metal alkoxide and the subsequent release of water triggers hydrolysis and condensation. Spontaneously formed hierarchically porous anatase titania monoliths have been prepared using a combination of sol–gel processing and phase separation, with colloidal titania as the metal oxide source and poly(ethylene oxide) as the phase separation inducer. By activating phase separation in parallel to gelation, a bicontinuous structure is formed. Careful variation of the titania and poly(ethylene oxide) concentrations permits control over the pore size and volume.[51] One problem these authors encountered was the use of colloidal titania as a starting material. The interparticle bonding strength was weak and a freeze-drying process was necessary to maintain the porosity. However, this process made the monoliths easily friable. Use of an alkoxy-derived titanium source in place of anatase nanoparticles bypasses this effect and allows for the formation of more robust structures.[52] By combining the sol–gel method with mild hydrothermal treatment and subsequent calcination, mesoporous CeO_2, ZrO_2, HfO_2, and TiO_2 have been prepared.[53] A laurylamine hydrochloride/metal alkoxide modified with acetylacetone was employed to give mesoporous samples with typical pore diameters of 3 nm to 6 nm. Epoxide-assisted sol–gel processing has been employed to prepare microporous composites of NiO–SiO_2.[54] Relatively quick hydrolysis of the Ni aquo precursor complex occurs with the addition of nitric acid, leading to the formation of nickel hydroxide. Increasing the Ni/Si molar ratio allows for the formation of a mesoporous structure.

Hierarchically porous structures may also be prepared by taking advantage of the rich interface dynamics of immiscible solvents. Titania particles, formed *via* hydrothermal treatment at the interface of a water–dichloromethane mixture, will remain trapped at that interface in an attempt to reduce the interfacial energy. These particles act as precursors for the formation of hierarchical nanostructured TiO_2. The hydrothermal conditions cause the nanoparticles to coalesce, forming spherical emulsions which aggregate at the interfacial region due to interparticle interactions. An acidic environment promotes the growth of nanorods, with the nanoparticles acting as seeds for the wire formation. N_2 sorption measurements and electron microscopy show that the intra-agglomerated rutile nanorods possess a mesoporous structure.[55]

Some unusual routes to spontaneously porous materials have been reported. Chen and coworkers have recently reported the first template-free synthesis of hierarchically porous lanthanide oxide foams.[56] These take the form of lanthanide-organic coordination polymers prepared by the hydrothermal reaction of lanthanum ions (La^{3+}, Ce^{3+}, Pr^{3+}, Nd^{3+}, Sm^{3+}, and Eu^{3+}) with asparagine. The asparagine is transformed to aspartic acid, which acts as the ligand. This is an important step in the formation of these foams. Traditionally, foaming methods for the preparation of porous materials require the incorporation of air into a suspension of the desired material.[57] In this case, a kind of reverse Ostwald ripening process occurs. Initially, dense spherical particles are formed. After the release of some of the internal ligands, these spheres are hollowed out *via* the dissolution of the inner body of the sphere. Also of note is that the formation of coordination polymers using asparagine could not be extended to main group or transition metals, indicating the importance of the lanthanide ion structural properties.

Composite materials

Spontaneous processes discussed so far have, on the most part, used a thermal process to selectively dissolve a phase to vapor or solution, thereby creating porosity. An important alternative route is to selectively react a portion of a single-phase precursor, so that a second phase is created simultaneously with porosity. Early work on spontaneously-formed inorganic composites began with attempts to improve the hardness and fracture toughness of Al_2O_3-based metal-ceramic composites.[58,59] The mechanism remains widely utilized: a single-phase ternary oxide precursor is calcined and sintered, then heated in a hydrogen atmosphere to selectively leach one cation to metal. The loss of oxygen induces void space that may or may not collapse, depending on firing temperature. The order and temperature of preferential reduction for specific cations can be predicted by using an Ellingham diagram.[60] As the firing temperature increases, metal particles can coarsen and the pores disappear *via* sintering. Often, registry between the metal and oxide lattice can be observed.[61,62]

More recently, interfacial and catalytic properties have been investigated using partial hydrogen reduction. For easily-reduced metals, nanosized precipitates form at low temperatures (700 °C and below in 5% H_2) and remain below 20 nm in diameter. Surprisingly, the majority of the nanoparticles are completely encased in the oxide matrix (rather than lying on surfaces), and crystallographic pore registry is maintained despite the necessary rearrangement to accommodate the

precipitates. There are two key aspects of this microstructure: large amounts of intimately contacting area between the two phases, and often facile ingress/egress of the nanoparticles under redox cycling. High interfacial area has been utilized by embedding ferromagnetic nanoparticles in an antiferromagnetic matrix, leading to a pinning of the magnetic easy axis known as exchange bias. The first such study by Sort *et al.* found very small loop shifts (exchange bias field, $H_E < 10$ Oe) after reducing a mixed $(Fe,Cr)_2O_3$ powder to Fe/Cr_2O_3.[63]

Using as a precursor $(Ni,Mn)_3O_4$, a wide composition range from Mn_3O_4 to $NiMn_2O_4$ can be accessed (see Fig. 10), and by reducing pellets to Ni/MnO, we have been able to tune H_E by many hundred Oe.[64] This approach is equally viable in bulk and thin film geometries (see Fig. 8),[47] and can be engineered for virtually any pair of transition metal cations: most commonly the ferromagnetic component is Fe, Co, Ni, or Fe_3O_4, while the antiferromagnet is α-Fe_2O_3, CoO, NiO, or MnO.[65] Alternatively, the composite can be prepared by direct reduction of the organic precursors, thereby eliminating the intermediate solid-solution oxide.[66]

Another example of the spontaneous development of biphasic architectures is in the realm of so-called "intelligent" catalysts.[67] Here, oxide hosts, such as perovskites, are host to noble metal ions under oxidizing conditions.[68] Incorporation of noble metals into a perovskite structure can prevent their sintering, reduce losses due to volatization at high operating temperatures, and avoid reactions with the support that lead to catalyst deactivation.[69] Under reducing conditions, the noble metal ions are released in the form of small particles, which are proposed to be catalytically active. Under conditions where the particles would sinter and lose surface area, they are re-absorbed into the perovskite lattice. Li *et al.* have reported a new systems capable of stabilizing Pd^{2+} in relatively large quantities, nearing 10 atm%, in the B-site of the perovskite and related structures.[68,70] The ability to incorporate such significant amounts of noble metal into the oxide host allow the process of redox cycling of noble metal (here Pd) nanoparticles in and out of the host. Fig. 11 shows a TEM image of the two-phase product of oxide and Pd nanoparticles that form upon reduction of $YFe_{1-x}PdO_{3-\delta}$ ($x = 0.10$). This substituted host oxide has the hexagonal $YAlO_3$ structure, rather than the more usual $GdFeO_3$ perovskite structure, the stability of hexagonal variant being imparted by the propensity of Pd to avoid octahedral coordination. Because Pd is the highest Z-number element in the mix, the two phase product allows Pd nanoparticles to be clearly seen in electron microscopy.[70]

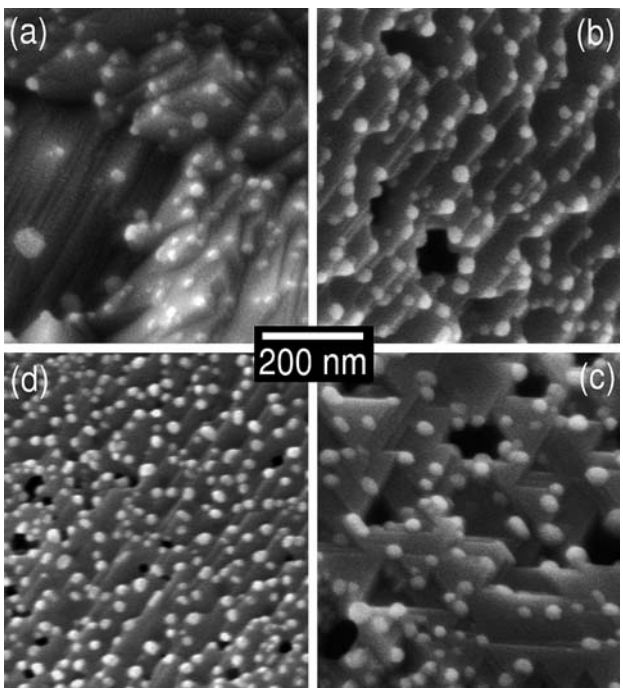

Fig. 10 (a–d) SEM images of Ni nanoparticles on an MnO matrix, produced by the hydrogen reduction of single-phase spinel $Mn_{3-x}Ni_xO_4$ samples as described in ref. 64. The density of Ni nanoparticles seems to change depending on the crystallographic face. Note the MnO matrix is itself porous.

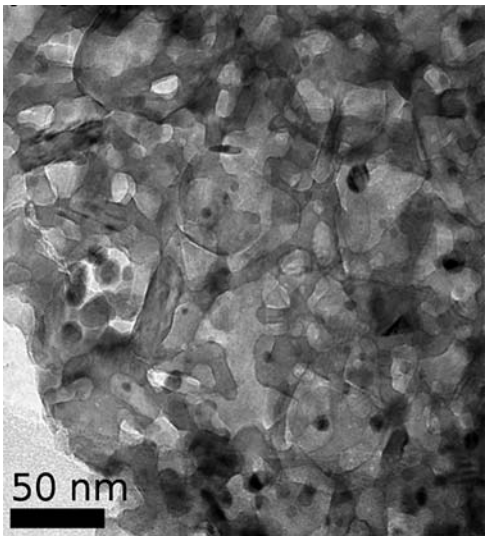

Fig. 11 Two-phase porous composites formed upon reduction of $YFe_{1-x}PdO_{3-\delta}$ ($x = 0.10$), showing Pd nanoparticles observed in transmission electron microscope as dark, approximately 10 nm-sized spheres. Reproduced with permission from ref. 70. © 2008, American Chemical Society.

Summary and outlook

A number of spontaneous processes in the solid state can be harnessed in the creation of porous materials. Many of these processes start with monolithic materials that transform to other monolithic materials in a process that is associated with loss of volume, which can be kinetically trapped to render the product monolith porous. The loss of volume can arise because a part of the initial monolith is volatilized, such as what is seen in the conversion of Mn_2O_3 or Mn_3O_4 to MnO. It can also arise because a sacrificial second phase, such as ZnO, is leached away. The final monolith is metastable in the sense that the thermodynamic preference would be for a dense rather than a perforated monolith. However, the rather slow diffusion of cations in the solid state prevents the pore walls from closing over. In many of the examples presented here, the final porosity occurs as perforated single crystals where the pore walls are actually the stable,

low energy surfaces of the crystals, for example, the {100} faces of rock salt MnO. A material with this sort of porosity is likely to be extremely stable against sintering and densifying at elevated temperatures, since the densification would not involve the elimination of grain boundaries. While none of the methods described here result in regular pores on a lattice, as seen with templated porous materials, the fact that the pore walls are crystallographic can permit the orientation of pores to be controlled.

It remains to be seen whether the new architectures with their associated methods of preparation will permit improved functionality once incorporated into new devices. However, as described in the last section on composite materials, the methods are already playing a role in development of unusual magnetic and catalytic systems. The key observation that emerges from many of the examples presented here is that a variety of simple and elegant solid-solid and solid-gas reactions can yield exquisitely intricate material architectures.

Acknowledgements

This work was principally supported by the donors of the Petroleum Research Fund of the American Chemical Society. SAC thanks Air Products & Chemicals, Inc. and the UC Discovery program for financial support. EST thanks the Beckman Foundation for a post-doctoral fellowship.

References

1 M. Tiemann, *Chem.–Eur. J.*, 2007, **13**, 8376.
2 F. Xu, P. Zhang, A. Navrotsky, Z.-Y. Yuan, T.-Z. Ren, M. Halasa and B.-L. Su, *Chem. Mater.*, 2007, **19**, 5680.
3 J. Yu, Y. Su and B. Cheng, *Adv. Funct. Mater.*, 2007, **17**, 1984.
4 M. Liu, G.-J. Zhang, Z.-R. Shen, P.-C. Sun, D.-T. Ding and T.-H. Chen, *Solid State Sci.*, 2009, **11**, 118.
5 Y.-J. Han, J. M. Kim and G. D. Stucky, *Chem. Mater.*, 2000, **12**, 2068.
6 P. Yang, T. Deng, D. Zhao, P. Feng, D. Pine, B. F. Chmelka, G. M. Whitesides and G. D. Stucky, *Science*, 1998, **282**, 2244.
7 F. C. Meldrum and R. Seshadri, *Chem. Commun.*, 2000, 29.
8 W. Yue, R. J. Park, A. N. Kulak and F. C. Meldrum, *J. Cryst. Growth*, 2006, **294**, 69.
9 Q. Dong, H. Su, F. Song, D. Zhang and N. Wang, *J. Am. Ceram. Soc.*, 2007, **90**, 376.
10 Q. Dong, H. Su, W. Cao, D. Zhang, Q. Guo and Y. Lai, *J. Solid State Chem.*, 2007, **180**, 949.
11 L. Zou, F. Li, X. Xiang, D. G. Evans and X. Duan, *Chem. Mater.*, 2006, **18**, 5852.
12 H. Niu, Q. Yang, K. Tang and Y. Xie, *Scr. Mater.*, 2006, **54**, 1791.
13 B. Tian, X. Liu, H. Yang, S. Xie, C. Yu, B. Tu and D. Zhao, *Adv. Mater.*, 2003, **15**, 1370.
14 J.-H. Smått, C. Weidenthaler, J. B. Rosenholm and M. Lindén, *Chem. Mater.*, 2006, **18**, 1443.
15 J.-H. Smått, N. Schüwer, M. Järn, W. Lindner and M. Lindén, *Microporous Mesoporous Mater.*, 2008, **112**, 308.
16 B.-L. Su, A. Léonard and Z.-Y. Yuan, *C.R. Chimie*, 2005, **8**, 713.
17 H. Zhang, G. C. Hardy, Y. Z. Khimyak, M. J. Rosseinsky and A. I. Cooper, *Chem. Mater.*, 2000, **14**, 4245.
18 H. Zhang, G. C. Hardy, M. J. Rosseinsky and A. I. Cooper, *Adv. Mater.*, 2003, **15**, 78.
19 R. Yuan, X. Fu, X. Wang, P. Liu, L. Wu, Y. Xu, X. Wang and Z. Wang, *Chem. Mater.*, 2006, **18**, 4700.
20 J. Zhu, O. K. Tan, Y. C. Lee, T. S. Zhang, B. Y. Tay and J. Ma, *Nanotechnology*, 2006, **17**, 5960.
21 Y. Yamauchi and K. Kuroda, *Chem.–Asian J.*, 2008, **3**, 664.
22 E. S. Toberer and R. Seshadri, *Chem. Commun.*, 2006, 3159.
23 P. Levitz, G. Ehret, S. K. Sinha and J. M. Drake, *J. Chem. Phys.*, 1991, **95**, 6151.
24 M. Panda, M. Rajamathi and R. Seshadri, *Chem. Mater.*, 2002, **14**, 4762.
25 M. Rajamathi, S. Thimmaiah, P. E. D. Morgan and R. Seshadri, *J. Mater. Chem.*, 2001, **11**, 2489.
26 E. S. Toberer, A. Joshi and R. Seshadri, *Chem. Mater.*, 2005, **17**, 2142.
27 M. Panda, R. Seshadri and J. Gopalakrishnan, *Chem. Mater.*, 2003, **15**, 1554.
28 E. S. Toberer, J. C. Weaver, K. Ramesha and R. Seshadri, *Chem. Mater.*, 2004, **16**, 2194.
29 B. Wang, *J. Am. Ceram. Soc.*, 2008, **91**, 4118.
30 Y. Liu and M. Liu, *Adv. Eng. Mater.*, 2006, **8**, 89.
31 L. Zou, X. Xiang, J. Fan and F. Li, *Chem. Mater.*, 2007, **19**, 6518.
32 Y. Suzuki, T. Yamada, S. Sakakibara and T. Ohji, *Ceram. Eng. Sci. Proc.*, 2000, **21**, 19.
33 Y. Suzuki, P. E. D. Morgan and T. Ohji, *J. Am. Ceram. Soc.*, 2000, **83**, 3185.
34 Z. Liu, T. Yamazaki, Y. Shen, D. Meng, T. Kikuta, N. Nakatani and T. Kawabata, *J. Phys. Chem. C*, 2008, **112**, 1391.
35 M. Paulose, C. A. Grimes, O. K. Varghese and E. C. Dickey, *Appl. Phys. Lett.*, 2002, **81**, 153.
36 M. RANEY®, US Patent, 1628190, 1927.
37 J. Erlebacher, M. J. Aziz, A. Karma, N. Dimitrov and K. Sieradzki, *Nature*, 2001, **410**, 450.
38 Y. Ding and J. Erlebacher, *J. Am. Chem. Soc.*, 2003, **125**, 7772.
39 L.-Y. Chen, J.-S. Yu, T. Fujita and M.-W. Chen, *Adv. Funct. Mater.*, 2009, **19**, 1221.
40 S. A. Corr, M. Grossman, J. D. Furman, B. C. Melot, A. K. Cheetham, K. R. Heier and R. Seshadri, *Chem. Mater.*, 2008, **20**, 6396.
41 D. P. Shoemaker, S. A. Corr and R. Seshadri, *Mater. Res. Soc. Symp. Proc.*, 2009, **1148E**.
42 E. S. Toberer and R. Seshadri, *Adv. Mater.*, 2005, **17**, 2244.
43 E. S. Toberer, J. Löfvander and R. Seshadri, *Chem. Mater.*, 2006, **18**, 1047.
44 E. S. Toberer, PhD thesis, *Spontaneous transformations in the solid state: Towards porous and biphasic materials*, University of California, 2006.
45 E. S. Toberer, T. D. Schladt and R. Seshadri, *J. Am. Chem. Soc.*, 2006, **128**, 1462.
46 E. S. Toberer, J. D. Epping, B. F. Chmelka and R. Seshadri, *Chem. Mater.*, 2006, **18**, 6345.
47 E. S. Toberer, M. Grossman, T. Schladt, F. F. Lange and R. Seshadri, *Chem. Mater.*, 2007, **19**, 4833.
48 T.-Z. Ren, Z.-Y. Yuan, W. Hu and X. Zou, *Microporous Mesoporous Mater.*, 2008, **112**, 467.
49 J. Yu, L. Zhang, B. Cheng and Y. Su, *J. Phys. Chem. C*, 2007, **111**, 10582.
50 M.-C. Tsai, J.-C. Chang, H.-S. Sheu, H.-T. Chiu and C.-Y. Lee, *Chem. Mater.*, 2009, **21**, 499.
51 J. Konishi, K. Fujita, K. Nakanishi and K. Hirao, *Chem. Mater.*, 2006, **18**, 864.
52 J. Konishi, K. Fujita, K. Nakanishi and K. Hirao, *Chem. Mater.*, 2006, **18**, 6069.
53 S. Pavasupree, Y. Suzuki, S. Pivsa-Art and S. Yoshikawa, *Sci. Technol. Adv. Mater.*, 2005, **6**, 224.
54 H. Cui and W. Ren, *J. Sol-Gel Sci. Technol.*, 2008, **47**, 360.
55 C. Wang, C. Shao, Y. Liu and X. Li, *Inorg. Chem.*, 2009, **48**, 1105.
56 Z. Shen, G. Zhang, H. Zhou, P. Sun, B. Li, D. Ding and T. Chen, *Adv. Mater.*, 2008, **20**, 984.
57 A. R. Studart, U. T. Gonzenbach, E. Tervoort and L. J. Gauckler, *J. Am. Ceram. Soc.*, 2006, **89**, 1771.
58 E. Breval, Z. Deng, S. Chiou and C. G. Pantano, *J. Mater. Sci.*, 1992, **27**, 1464.
59 C. Laurent, J. J. Demai, A. Rousset, K. R. Kannan and C. N. R. Rao, *J. Mater. Res.*, 1994, **9**, 229.
60 W. W. Smeltzer and D. J. Young, *Prog. Solid State Chem.*, 1975, **10**, 17.
61 S. Suenaga, T. Suetsuna, K. Harada and T. Fukasawa, *J. Am. Ceram. Soc.*, 2004, **87**, 963.
62 T. Suetsuna, T. Fukasawa, S. Suenaga and K. Harada, *J. Am. Ceram. Soc.*, 2007, **90**, 3441.
63 J. Sort, V. Langlais, S. Doppiu, B. Dieny, S. Surinach, J. S. Munoz, M. D. Baro, Ch. Laurent and J. Nogués, *Nanotechnology*, 2004, **15**, S211.

64 D. P. Shoemaker, M. Grossman and R. Seshadri, *J. Phys.: Condens. Matter*, 2008, **20**, 195219, 195219–1–9.
65 J. Nogués, J. Sort, V. Langlais, V. Skumryev, S. Suriñach, J. S. Muñoz and M. D. Baró, *Phys. Rep.*, 2005, **422**, 65.
66 Kumar and K. Mandal, *J. Appl. Phys.*, 2007, **101**, 113906–5.
67 Y. Nishihata, J. Mizuki, T. Akao, H. Tanaka, M. Uenishi, M. Kimura, T. Okamoto and N. Hamada, *Nature*, 2002, **418**, 164.
68 J. Li, U. G. Singh, J. W. Bennett, K. Page, J. C. Weaver, J.-P. Zhang, T. Proffen, A. M. Rappe, S. L. Scott and R. Seshadri, *Chem. Mater.*, 2007, **19**, 1418.
69 U. G. Singh, J. Li, J. W. Bennett, A. M. Rappe, R. Seshadri and S. L. Scott, *J. Catal.*, 2007, **249**, 349.
70 J. Li, U. G. Singh, T. D. Schladt, J. K. Stalick, S. L. Scott and R. Seshadri, *Chem. Mater.*, 2008, **20**, 6567.

